Electrochemical and molecular modelling studies of CO_2 corrosion inhibition characteristics of alkanolamine molecules for the protection of 1Cr steel

Gupta, Shivangi; Gupta, Kapil Kumar; Andersson, Martin; Yazdi, Rouhollah; Ambat, Rajan

Published in:
Corrosion Science

Link to article, DOI:
10.1016/j.corsci.2021.109999

Publication date:
2022

Document Version
Publisher's PDF, also known as Version of record

Corrosion Science 195 (2022) 109999

Contents lists available at ScienceDirect

Corrosion Science

journal homepage: www.elsevier.com/locate/corsci

Electrochemical and molecular modelling studies of CO_2 corrosion inhibition characteristics of alkanolamine molecules for the protection of 1Cr steel

Shivangi Gupta [a,*], Kapil Kumar Gupta [a], Martin Andersson [b], Rouhollah Yazdi [a], Rajan Ambat [a]

[a] Section of Materials and Surface Engineering, Department of Mechanical Engineering, Technical University of Denmark, Produktionstorvet, 2800 Kongens Lyngby, Denmark

[b] Department of Chemical Engineering, Technical University of Denmark, Produktionstorvet, Kongens Lyngby 2800, Denmark

ARTICLE INFO

Keywords:
A. Steel
B. Polarization
B. EIS
B. XPS
B. modelling studies

ABSTRACT

Effects of alkanolamine molecules on the corrosion inhibition of L80–1Cr steel were studied in a CO_2-saturated 1 wt% NaCl solution at well downhole temperatures of 20 and 80 °C. The electrochemical results showed lower corrosion rates at 20 °C, for which corrosion rates were more influenced by the alkanolamine injection. The experimental results and molecular modelling calculations using DFT revealed that alkanolamine adsorption/desorption played a determining role in the kinetics and characteristics of $FeCO_3$ formation. Additionally, the dependency of inhibitor efficiency on both chemical structures and adsorption energy on Fe(110), $FeCO_3$(104) and Fe_3C(001) was demonstrated, resulting in the highest efficiency provided by ethanolamine.

1. Introduction

Despite their susceptibility to CO_2 corrosion, carbon and low alloy steels are the most commonly used materials in oil and gas production/transmission infrastructure; due to their relatively low price, availability, mechanical characteristics, ease of use in construction, and economic effectiveness by corrosion inhibition [1]. When CO_2 dissolves in water and hydrates to carbonic acid (H_2CO_3), it promotes electrochemical reactions between the steel surface and the aqueous phase, leading to iron dissolution [2–7]. In some circumstances, corrosion products or mineral scales can precipitate on the surface, which likely has a significant influence on the corrosion mechanism(s). This electrochemical process has been under investigation for more than four decades, but the corrosion mechanisms occurring at the metal-electrolyte interface are still the main subject of research [8,9].

Iron carbonate formation in the form of siderite ($FeCO_3$) is the most commonly observed corrosion product in an aqueous NaCl-containing medium saturated with CO_2. This has been proved to be one of the most important factors governing the rate of corrosion [1,10]. The influence of this layer on the corrosion rate of steel has been researched and documented in the literature [11–15]. Indeed, the iron carbonate layer can slow the general corrosion process by acting as a physical barrier to the diffusion of ionic species involved, covering up a portion of the steel surface, and preventing the underlying steel from further dissolution. In other words, under certain conditions, $FeCO_3$ precipitation on the steel surface blocks the active sites of dissolution and creates a barrier to the diffusion of the electrochemically active species, resulting in a significant reduction in the corrosion rate. Iron carbonate layer growth depends primarily on the kinetics of the electrochemical reactions. As more iron carbonate precipitates, the layer grows in a higher density and thickness. However, the steel surface continuously corrodes under the layer, creating "voids" between the layer and the steel surface. When the rate of precipitation at the steel surface equals or exceeds the rate of corrosion, dense, protective layers form, which are sometimes very thin but still protective. The opposite scenario occurs when the corrosion process undermines the newly formed layer faster than precipitation can fill in the voids, and a porous and unprotective layer forms which can be sometimes very thick [16].

The protectiveness of the iron carbonate layer is strongly dependent on several parameters such as CO_2 partial pressure [11–14], concentration of ionic species [17,18], pH and temperature [19–22]. Temperature is one of the most crucial parameters that influences the corrosion of mild steel in CO_2 environments. At low pH values (when the solubility of $FeCO_3$ is high), an increase in temperature accelerates both the mass transport in the bulk solutions and the kinetics of chemical and electrochemical reactions at the metal-electrolyte interface. This leads to an

* Corresponding author.
E-mail address: shig@mek.dtu.dk (S. Gupta).

https://doi.org/10.1016/j.corsci.2021.109999
Received 30 June 2021; Received in revised form 21 November 2021; Accepted 29 November 2021
Available online 1 December 2021

increase in the corrosion rate [23,24]. The peak in the corrosion rate has been reported in the literature to be between 60 °C and 80 °C [20–22]. Below ~ 60 °C, no protective layer is formed and the corrosion products are porous and not well adherent to the steel surface. At temperatures higher than about 60 °C, the $FeCO_3$ layer becomes denser and more adherent to the surface, creating a solid barrier between the metal and the electrolyte, which reduces the corrosion rate of the steel [25–29].

Due to the formation of various corrosion products with unpredictable and uncertain levels of protectiveness, the use of corrosion inhibitors is considered as one of the suitable and economical methods for reliable production of oil and gas [30,31]. The addition of corrosion inhibitors effectively secures the metal against an acid attack. Inhibitors on the metal surface mainly act as a competitive absorbant against the aggressive ions. The adsorption on the metal surface is influenced by the surface nature and its charge-transfer properties, the type of aggressive electrolyte, and the chemical structure of inhibitors [32]. Most inhibitors are organic molecules possessing N, S, P and O hetero-atoms. There are different types of inhibitors of which organic corrosion inhibitors are mostly applied in the oil and gas industry. The organic corrosion inhibitors are layer-forming agents and are usually adsorbed on the surface of metals through a physical or chemical process. The mechanism of adsorption of most corrosion inhibitors can be understood by the determination of the adsorption properties of organic corrosion inhibitors [33]. The adsorption energy of inhibitor molecules can be calculated at the electronic level using Density Functional Theory (DFT). Most of the commercial organic corrosion inhibitors comprise of N-containing molecules amines, quarts, imidazoline, etc. which effectively adsorb on the metal surface and inhibits the corrosion processes. There are various factors which influence the adsorption and efficiency of corrosion inhibitors, such as the molecular structure of the inhibitors, inhibitor concentration, exposure time, electrolyte chemistry, temperature of the system, etc. [34].

Despite the existence of several studies, discussing the inhibitive effects of N- containing organic molecules on mild steel [35,36], the atomic interaction of the inhibitors with the steel surface is still unclear in the present literature especially when iron carbonate is formed at high temperatures. Thus, it is an important subject to understand whether amine-based corrosion inhibitors have a complementary effect on iron carbonate or are detrimental to its formation. The aim of this comprehensive study is to investigate the effect of amine-based organic corrosion inhibitors on bare 1Cr steel and the pre-formed $FeCO_3$ using electrochemical techniques as well as molecular modelling. In addition, inhibitor injection frequency experiments were studied to understand the role of the application method in corrosion mitigation. For this purpose, the electrochemical behavior of steel grade L80–1Cr has been investigated at 20°C and 80°C, the typical temperatures of oil production wells of the Danish sector of the North Sea. To assess the electrochemical behavior of the material and to measure corrosion rate, different electrochemical techniques such as Open Circuit Potential (OCP), Linear Polarization Resistance (LPR) and Electrochemical Impedance Spectroscopy (EIS) were used. Furthermore, for a comprehensive understanding of the inhibitor adsorption mechanism, different surface characterization techniques, including Scanning Electron Microscopy (SEM) equipped with Energy Dispersive Spectroscopy (EDS), and X-ray Photoelectron Spectroscopy (XPS) were employed.

2. Material and methods

2.1. Material and specimen preparation

The specimens used in this study were made of a martensitic 1Cr steel (L80) in the quenched & tempered condition with a chemical composition listed in Table 1. The specimens were machined into a cylindrical shape with a total surface area of 3.95 cm^2. The surface of the specimens was mechanically polished with SiC papers up to P1000 grade. Immediately after polishing, the specimens were degreased using ethanol, rinsed with de-ionized water, and then air-dried. The dried specimens were then mounted on a specimen holder and immersed in the test solution. At the end of the tests, the specimens were immediately retrieved, rinsed with ethanol, dried in air and stored in a desiccator for further assessments.

Table 1
Chemical composition in wt% of the L80–1 Cr steel.

Material	C	Cr	Mn	Mo	P	Si	S	Fe
API 5CT L80 – 1Cr Steel	0.40	1.10	0.75	0.20	≤ 0.035	0.20	≤ 0.040	base

2.2. Electrolyte preparation

The electrochemical experiments were conducted on the 1Cr steel samples in a CO_2-saturated 1 wt% NaCl solution at 20 °C and 80 °C. Before immersing the specimen in the solution, the electrolyte was sparged with nitrogen for about 12 h to deoxygenate. The gas was then switched to CO_2 and bubbled for 4 h in order to saturate the solution. After gas bubbling, the pH of the solution was measured to be 3.9 for 20 °C and pH 4.2 for 80 °C. Three alkanolamines (possessing alcohol and amine functional groups) including ethanolamine, diethanolamine and triethanolamine with pKa values (at 25 °C) of 9.5, 8.88, 7.8, respectively, were used in the current study. An amount of 200 parts per million by volume (ppm_v) of inhibitors was injected into the solution. After inhibitor injection and before the immersion of the bare 1Cr steel samples, the solution was de-aerated again for at least 30 min in order to remove possible trapped oxygen during the injection. In another phase of this work, in order to study the effects of the inhibitors on the iron carbonate layer, $NaHCO_3$ was added to adjust the pH of the solution to 6.5 in order to facilitate iron carbonate precipitation prior to the alkanolamines injection. After pH adjustment, the solution was again de-aerated for at least one hour with CO_2 gas bubbling. During testing, CO_2 gas was continuously bubbled to the solution to maintain its saturation and avoid any oxygen entrance.

2.3. Electrochemical and weight loss measurements

The corrosion tests were carried out in an airtight 1.5 L glass container using a standard three-electrode cell. An Ag/AgCl reference electrode was placed in contact with the solution through a glass-luggin capillary and a concentric platinum wire ring was used as the counter electrode. The corrosion potential (E_{corr}) was monitored and the linear polarization resistance (LPR) was measured every 1.5 h. During LPR measurements, the potential was scanned in a potential range of ± 10 mV vs. open-circuit potential (OCP) at a scan rate of 0.167 mV/s. Based on our previous experience, a duration of 1 h was chosen for the system to stabilize the initial OCP. After the OCP stabilization, the EIS measurements were performed by applying an AC signal amplitude of 10 mV vs OCP in a frequency range of 10 mHz – 10 kHz.

The weight loss method was employed to calculate the corrosion rate for the steel samples in the CO_2-saturated 1 wt% NaCl solution without and with alkanolamines injection at 20 and 80 °C after 24 hr. For this purpose, after rinsing and drying, the initial weight of pre-immersed specimens was measured by a calibrated weighing tool with the accuracy of 10^{-5} gr. After the immersion tests, the corrosion products on the surface, if any, were removed using Clark's solution in accordance with the standard procedure mentioned in ASTM G1–03, and then the final weight and weight loss were (W) obtained. The corrosion rate was eventually obtained based on the following equation:

$$Corrosion\quad rate\quad \left(mm\Big/yr\right) = 8.76\times 10^{4}\frac{W}{A.T.D} \tag{1}$$

where "W" is mass loss in grams; "T" is time of exposure in hour, "A" is the exposing surface area in cm^2, and "D" is density in gr/cm^3.

2.4. Experimental conditions and procedure

As listed in Table 2, initially, the effect of the alkanolamines on L80–1 Cr steel at two temperatures of 20 °C and 80 °C was studied in the CO_2-saturated electrolyte. A 200 ppm_v concentration of the alkanolamine was injected into the solution at the beginning of the experiment and then electrochemical experiments were conducted. To understand the injection frequency of the inhibitors, another set of experiments was carried out in the NaCl solution in which the alkanolamines were intermittently injected to observe their effects on the corrosion behavior of L80–1 Cr steel. In this strategy, three different procedures were established as shown in Fig. 1a. In case I, the 200 ppm_v inhibitor was initially injected before immersing the sample in the solution. In case II, the same amount of inhibitor was injected after 12 hrs of the immersion, which means that the sample was pre-corroded for 12 hrs. In case III, a two-time injection of the inhibitors was done; (1) initial injection, 30 min before electrochemical measurements and, (2) final injection after 12 hrs of electrochemical measurement. All electrochemical experiments were performed at least twice and the average values with error bars are reported in the Results section.

As iron carbonate is the main corrosion product that may form over the steel material in a CO_2 environment, therefore, the inhibitive effect of alkanolamines on iron carbonate formation was also studied. For this purpose, two injection frequency cases were selected as shown in Fig. 1b. In the first case, the sample was anodically polarized with the current density of 61.1 μA/cm^2 in the NaCl solution at 80 °C and pH 6.5 for 24 hrs in order to accelerate Fe^{2+} ion dissolution into the solution. Then, the alkanolamines were injected under the OCP conditions to observe how they influence the formation and growth of $FeCO_3$. In the second, after the anodic polarization, the OCP condition was applied on the sample in the solution for 24 hrs before injecting the alkanolamines. This enables the system to get saturated with Fe^{2+} ions and as a result, $FeCO_3$ was formed on the surface. Then, the effect of the alkanolamines on the corrosion behavior of the pre-formed $FeCO_3$ layer was studied. After each experiment, the samples were cleaned in deionized water, flushed with ethanol and air-dried. All samples were stored in a desiccator before further characterization analyses.

2.5. Surface characterization and phase analysis

The morphological and elemental analysis of the corrosion products were investigated using a Zeiss Supra FEG-SEM using 20 kV acceleration voltage, assisted with Energy Dispersive X-ray spectroscopy (EDS) analysis equipment. Grazing Incidence X-Ray Diffraction (GIXRD) was also used to determine the phase composition of the formed layer using a Bruker D8 Advance. The instrument was operated at 35 kV and 50 mA with Cr-Kα radiation (λ = 0.22909 nm). The incidence angle was 3° and the 2θ ranged was selected from 35° to 85°, with the step size of 0.05°, and a 10 s count time at each step.

X-ray photoelectron spectroscopy (XPS) spectra were recorded using a commercial XPS-Thermo Scientific system. The base pressure in the experimental chamber was below 10^{-9} mbar. The spectra were collected using Al Kα X-ray source (1486.6 eV) radiation and the overall energy resolution was about 0.8 eV. High-resolution scans with 0.1 eV steps were conducted over the following regions of interest: C 1 s, N 1 s and O 1 s. Surface charging effects were compensated by referencing the binding energy (BE) to the C 1 s line of residual carbon set at 285.0 eV BE. XPS spectra were deconvoluted using a non-linear least-squares algorithm with a Shirley baseline and a Gaussian–Lorentzian combination. Thermo Avantage software, version 5.9913, was used for all XPS data processing.

Table 2
Experimental conditions of electrochemical experiments used in this study.

Parameter	Condition
Material	1Cr steel
Solution	1 wt% NaCl in Deionized water, CO_2 Saturated
Temperature	20 °C and 80 °C
CO_2 partial pressure	0.98 bar at 20 °C and 0.53 bar at 80 °C
Rotation	300 rpm
Inhibitor concentration	200 ppm_v
Test duration	24 and 72 hrs

2.6. Computational details

The DFT calculations were performed in a pseudopotential plane-wave formalism with the Quantum Espresso package [37]. The adsorption energies for water, ethanolamine, diethanolamine and triethanolamine on a Fe(110) surface and a $FeCO_3$(104) surface were calculated to model the different behavior of water and the alkanolamines on pristine and CO_2 corroded iron. The adsorption energy of ethanolamine was also calculated on a Fe_3C(001) surface.

To perform slab calculations on Fe(110), $FeCO_3$(104) and Fe_3C(001), 15–20 Å of vacuum between the material slabs was inserted. The slabs for each of the materials consisted of four molecular layers. The fourth molecular layer (furthest from the side of the adsorbates) was frozen during the geometry optimizations. The lattice parameters used for each material were found by optimizing the cell parameters for the corresponding bulk material, using the same pseudopotentials, exchange-correlation functional that was later used for calculating adsorption energies, in order to minimize the effects of surface strain on adsorption properties. For $FeCO_3$(104), only the gamma point was used during geometry optimizations, for Fe(110) a 4×4x1 k-point sampling was used and for Fe_3C(001) a 6×6x1 k-point sampling was used. The revPBE functional [38] with added semi-empirical dispersion corrections were employed in the DFT-D2 implementation [39–41]. The s6 parameter for revPBE was 1.25, and a 12 Bohr cutoff was used for Fe calculations [39]. The C6 vdw parameters for Fe were reduced by a factor of 33 to take into account the decreased polarizability of cations when they are bonded within an ionic material [42–44]. All pseudopotentials were ultrasoft (US), Projector-Augmented Wave (PAW) and Norm-Conserving (NC) were generated using revPBE, and were taken from PS Library 0.2.5 [45, 46]. The kinetic energy cutoff was 40 Ry, and the density cutoff was 400 Ry, which has been shown for similar setups to provide converged adsorption energies [43,44].

In order to assess the specific molecular interaction with the model surfaces, the adsorption energy was calculated using Eq. (2).

$$E_{adsorption} = E_{surface+inhibitor} - (E_{surface}) - (E_{inhibitor}) \quad (2)$$

The dual functional groups of the alkanolamines allow for the adsorption with either group to the solid surfaces. The adsorption energies of both binding geometries were calculated. Using this convention, the more negative the adsorption energy, the stronger is the bond between the molecule and the surface.

3. Results

3.1. Molecular modelling simulation using density functional theory (DFT)

Amines contain a sp3 hybridized nitrogen atom on which another element or functional group can be bonded with three single bonds. Ethanolamine, commonly named monoethanolamine (MEA), is an organic chemical compound that has both primary amine and alcohol functionalities and acts as a weak base. All amines have a lone pair of electrons. However, the readiness with which the lone pair of electrons is available for co-ordination with a proton determines the basic strength of amines. The inhibitive effect of ethanolamine is achieved by donating the unshared pair of electrons from the nitrogen atom,

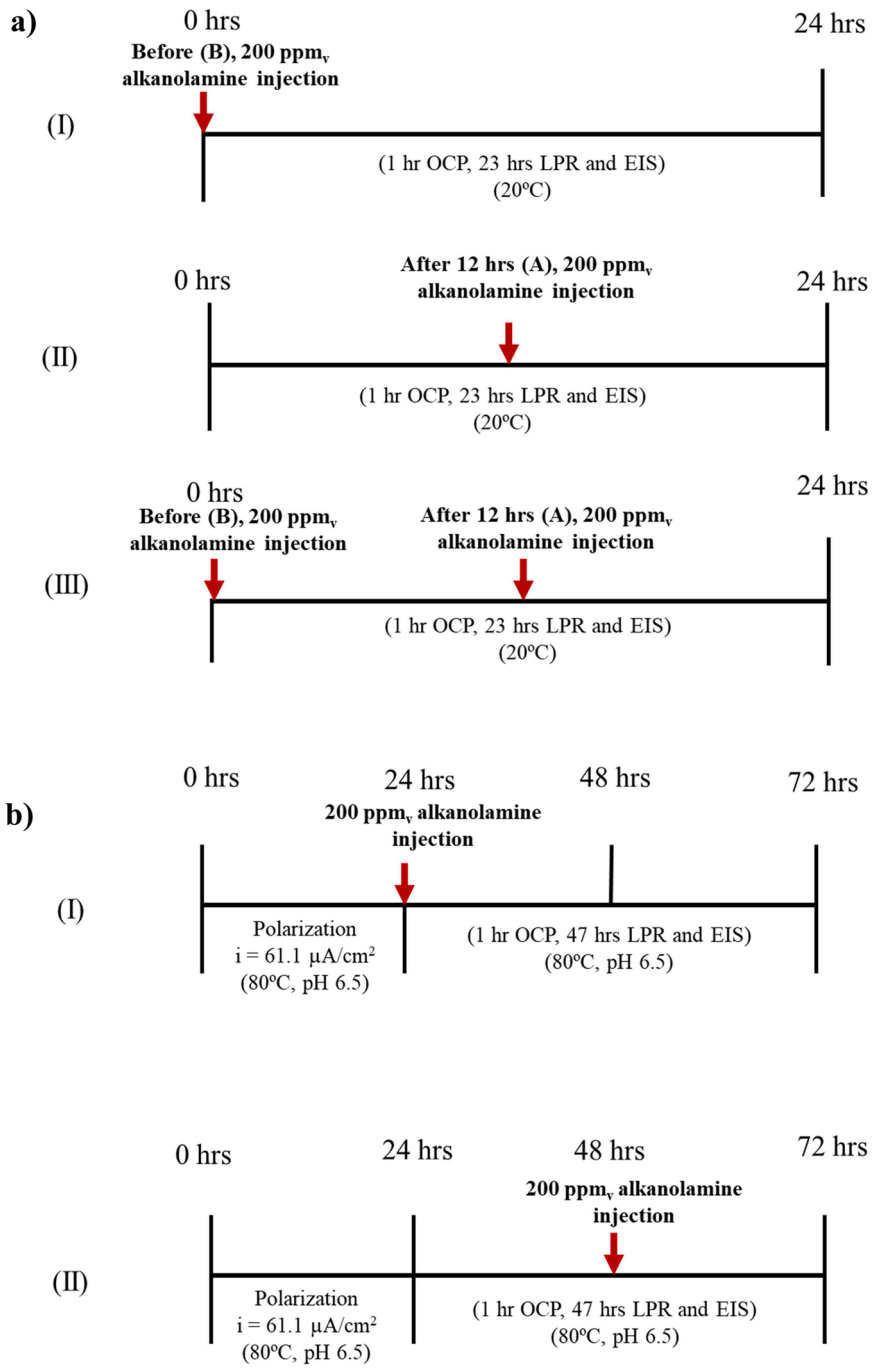

Fig. 1. . (a): Inhibitor injection frequency on L80- 1Cr steel, (b) Inhibitor injection frequency on the steel covered with iron carbonate ($FeCO_3$) corrosion products.

followed by a surface complex-forming [32]. Adsorption energy calculations using DFT were conducted to further study the interaction between tested inhibitors and Fe(110) and $FeCO_3$(104) stable surfaces in the gas phase. In Table 3, the calculated adsorption energies of the most stable bonding geometry of each alkanolamine on the surfaces are shown. When comparing the adsorption energy on Fe and $FeCO_3$ surfaces, water as well as all alkanolamines had more negative values for the $FeCO_3$ surface indicating a stronger bond. On Fe surfaces, however, water had the least negative (−31 kJ/mol) adsorption energy value representing the weakest bond with Fe surface in comparison to the alkanolamines. Among different alkanolamines, diethanolamine had the most negative adsorption energy value (−122 kJ/mol) on the Fe surface, thus formed the strongest bond. The adsorption energy value trend for the $FeCO_3$ surface was slightly different than the Fe surface. Water still had the least negative value (−106 kJ/mol); however, amongst the alkanolamines, ethanolamine and diethanolamine had more negative values (−152 and −151 kJ/mol, respectively) than triethanolamine.

The inhibitor adsorption energy was estimated in water by comparing the adsorption energy of the inhibitor with that of water in Table 3. This estimation is based on the fact that an inhibitor molecule needs to replace water molecule(s) already bonded at the interface. The size of the inhibitor molecule at the interface can govern either one or two water molecules need to be displaced from the surface. For ethanolamine, one water molecule was chosen, and for diethanolamine, however, a single and couple of water molecule(s) were selected for the -OH and -NH anchoring group, respectively.

Table 3
Adsorption energy values of the alkanolamines as the inhibitors and the difference in the adsorption energy of the alkanolamines and water ($\Delta E_{adsorption}$) on Fe(110), Fe_3C(001) and $FeCO_3$(104) surfaces using DFT (in kJ/mol).

Molecule	Anchoring group	$E_{adsorption}$ Fe (110)	$E_{adsorption}$ $FeCO_3$ (104)	$E_{adsorption}$ Fe_3C (001)
Water	−OH	− 31	− 106	− 62
Ethanolamine (C_2H_7NO)	$-NH_2$	− 84	− 152	− 125
	−OH	− 59	− 123	–
Diethanolamine ($C_4H_{11}NO_2$)	−NH	− 122	− 151	
	−OH	− 69	− 129	
Triethanolamine($C_6H_{15}NO_3$)	−N	[a]	− 141	
	−OH	− 73	− 134	

Differences in adsorption energy between inhibitor and water

Molecule	# water molecules replaced	Anchoring group	$\Delta E_{adsorption}$ Fe(110)	$\Delta E_{adsorption}$ $FeCO_3$(104)	$\Delta E_{adsorption}$ Fe_3C(001)
Ethanolamine (C_2H_7NO)	1	$-NH_2$	− 53	− 46	− 63
Diethanolamine ($C_4H_{11}NO_2$)	1	−OH	− 38	− 23	–
	2	−NH	− 60	+ 61	

[a] The chosen unit cell of the Fe(110) surface was too small to fit an N-bonded triethanolamine without artefacts from interactions with the periodic images.

3.2. Binding energy calculation using XPS at 20 °C

To confirm the assumption of the alkanolamine chemisorption and elucidate the nature of the organic thin-layer formed on the Fe surface, X-ray photoelectron spectroscopy (XPS) analyses were carried out. For comparison purposes, the XPS spectra as shown in Fig. 2 were obtained on the steel surfaces, which were previously immersed in the pure alkanolamines. All XPS spectra show complex forms, which were assigned to the corresponding species through a deconvolution fitting procedure. The high-resolution N 1 s spectrum of the sample treated by the alkanolamines shows the peaks indicative of the presence of different nitrogen-containing molecules on the steel surface. The deconvoluted N 1 s spectrum for pure ethanolamine shows two main peaks (Fig. 2a). The first peak located at approx. 397.0 eV has the largest contribution and is attributed to the coordinate nitrogen in ethanolamine bonded with the steel surface and the second peak at the binding energy of 399.5 eV corresponds to the bonds of C-N and the unprotonated N atoms in the ethanolamine structure. In Fig. 2b, the first peak is located at approx. 402.1 eV which is at a higher binding energy, attributed to positively charged nitrogen, and could be related to a protonated nitrogen atom (=N^+H−) in the diethanolamine structure. A similar trend has been observed in Fig. 2c for triethanolamine.

3.3. Electrochemical responses at 20 °C and 80 °C

3.3.1. LPR measurements

The results obtained from the LPR measurements (corrosion potential and polarization resistance) on 1Cr steel at the temperatures of 20 °C and 80 °C are shown in Fig. 3. The comparison of Figs. 3a and 3b shows that the evolution of the corrosion potential depends on the exposure temperature. In Fig. 3a, the samples tested in the alkanolamine-containing solution at 20 °C show different corrosion potential trends without a significant variation over the period of the experiment. Only the reference sample shows a slight OCP delay from − 630 mV to about − 650 mV, probably due to the breakdown of the pre-immersion, residual air-formed oxide film [47], leaving more active sites on the surface which somewhat increased the corrosion tendency of the sample. At 80 °C, however, the corrosion potential for all samples slightly increased with time (Fig. 3b), suggesting the formation of a protective layer by electrochemical redox reactions. For instance, the E_{corr} for the sample (i.e. reference sample) at 80 °C increased in the solution with ethanolamine injection from approximately − 660 mV to − 640 mV and then remained unchanged. In comparison, the injection of the alkanolamines resulted in a nobler corrosion potential for the steel sample, indicating a less thermodynamic tendency to corrosion.

The corrosion rates of the 1Cr steel samples in the uninhibited and inhibited conditions were acquired after 24 h of immersion in the solution at 20 and 80 ℃ based on the weight loss technique and are presented in Fig. 3e and f. The corrosion rates of the samples at 20 ℃ were

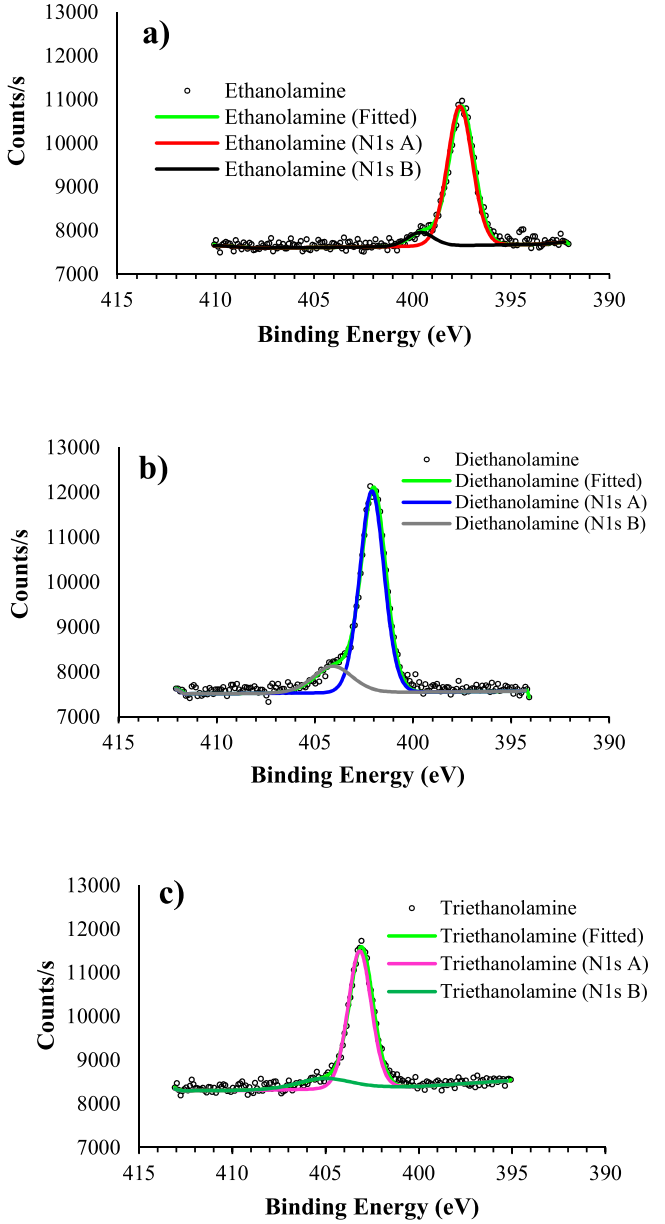

Fig. 2. The XPS deconvoluted profiles of N 1 s for pure (a): ethanolamine, (b): diethanolamine and (c): triethanolamine.

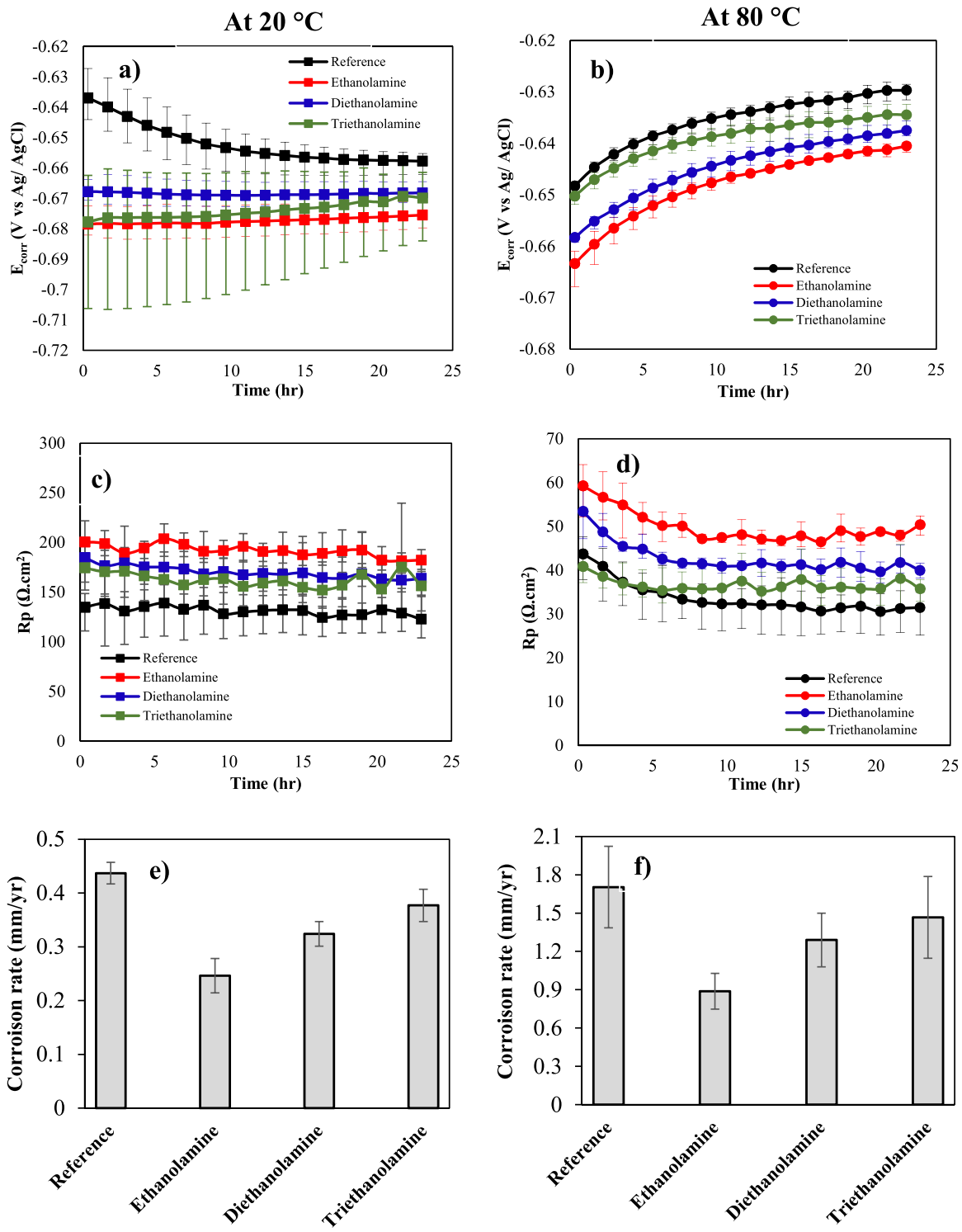

Fig. 3. Variations of: (a, b) E_{corr} as a function of time, (c, d) polarization resistance as a function of time, and (e, f) the corrosion rate (mm/yr) obtained by weight loss technique; for the L80–1 Cr steel samples in 1 wt% NaCl solution for 24 hrs without and with the addition of 200 ppmv of different alkanolamines at 20 °C and 80 °C, respectively.

about 4.4, 2.5, 3.2 and 3.8 mm/yr for the uninhibited sample and those inhibited by ethanolamine, ethanolamine and triethanolamine, respectively. Indeed, the results show a lower the corrosion rate for inhibited samples in Fig. 3e, which are found to be consistent with the higher final polarization in Fig. 3c. For instance, the polarization resistance of the reference sample as a function of time for L80–1 Cr steel at 20 °C in Fig. 3c shows an about constant corrosion resistance of 130 Ω.cm^2, whereas ethanolamine shows the highest resistance value (i.e., the lowest corrosion rate in Fig. 3e) of approx. 200 Ω.cm^2 corresponding to 70% increase in comparison to the reference sample. In addition, diethanolamine and triethanolamine exhibit a corrosion resistance of 170 Ω.cm^2 (60% increase) and 160 Ω.cm^2 (50% increase), respectively. Whereas, at 80 °C, both Rp values and corrosion rates reveal a comparably lower corrosion resistance even with the addition of the

alkanolamines see Fig. 3d and f. This means that the samples exposed to the amines-containing solution at the higher temperature show only 10–20% increase in corrosion resistance compared to the reference sample. The inhibition efficiency for the different alkanolamines at 20 CE 80 ℃ was calculated based on Eq. (3) and is listed in Table 4. The table confirms the lower efficiency of the inhibitors at the high temperature, which is likely attributed to the less controllable acceleration of electrochemical reactions.

$$\textbf{Inhibitor efficiency } (\%) = \frac{\left(R_{p\,\text{Inibited}} - R_{p\,\text{Uninhibited}}\right)}{R_{p\,\text{Inhibited}}} \times 100 \quad (3)$$

Due to the better corrosion inhibition of ethanolamine and diethanolamine in comparison to triethanolamine (Fig. 3c and d), it was also planned to study the injection frequency effect of these two alkanolamines on the corrosion behavior of the steel surface. Fig. 4 shows the LPR results of 1Cr steel at 20 °C. Two different frequency strategies were considered (see Fig. 4a and b). In the first case, when alkanolamines were injected after 12 h of corrosion, (Fig. 4a), the resistance value was sharply increased from about 125–185 and 170 Ω.cm^2 for ethanolamine and diethanolamine, respectively. In the second one, the alkanolamines were injected two times, (Fig. 5b) before starting the experiment and after 12 h of immersion. Despite the effective initial inhibition levels provided by the alkanolamines similar to the previous condition, the results in Fig. 4b show that there is no significant change in the resistance value when the alkanolamines were reinjected after12 hours. The polarization resistance is approximately 190 Ω.cm^2 for both ethanolamine and diethanolamine. The proposed mechanisms of inhibitions provided by the alkanolamines in the various injection frequencies will be discussed in the Discussion section.

During higher temperatures (60–80 °C), the possibility of iron carbonate formation in CO_2-saturated solutions increases [23,24], which sometimes protects the steel surface from further corrosion. Therefore, in the presence of the alkanolamines, their effect on the formation of iron carbonate products was also worth study. To form a $FeCO_3$ layer, it is important to maintain optimal temperature and pH conditions for the NaCl solution which were selected to be 80 °C and 6.5, respectively. The results from LPR measurements (polarization resistance) for the samples under these conditions are shown in Fig. 5. In Fig. 5a, when the alkanolamines were injected from the very beginning (just after polarization), the protectiveness provided by $FeCO_3$ formation was postponed to a longer immersion time (i.e., once there was a sharp increase in R_P value) as compared with the reference sample. In the reference sample, for example, the significant rise in the R_P value induced by the protective $FeCO_3$ formation starts after 4 hrs, however, the sample exposed to ethanolamine delayed by 26 hrs. Also by injecting diethanolamine and triethanolamine, the $FeCO_3$ layer was delayed to effectively protect the substrate by 6 and 14 hrs, respectively. In the other scenario, the sample was initially polarized at an anodic current density of 61.1 μA/cm^2 for 24 h to form a $FeCO_3$ layer (after 24 hrs) and then the alkanolamines were injected into the system. In Fig. 5b, it can be seen from the LPR trends that there is a small effect on the R_P value by alkanolamine injection, suggesting no significant inhibitor efficiency in this case.

3.3.2. Electrochemical impedance spectroscopy investigation

Fig. 6 presents the results of the EIS measurements of the samples in the solution without and with alkanolamine injection at 20 °C and 80 °C after 24 hrs immersion. The Nyquist plot for the samples exposed at 80 °C shows two incomplete and depressed semicircles, one at high-medium (HF-MF) frequencies and one at low frequencies (LF), which are partly overlapped with each other. Samples in alkanolamine-containing solutions show a higher diameter for both semicircles compared to the reference sample. Whereas, the Nyquist plot for the sample exposed to the solution at 20 °C in Fig. 6 presents one oval semicircle. At both temperatures, the diameter of the semicircles, which indicates the polarization resistance, is the highest for ethanolamine. The EIS results of the experiments at 20 °C and 80 °C were further analyzed using the numerical fitting with the most commonly used equivalent electrical systems related to corroding steel. The electrochemical system shown in Fig. 7a is a simple Randle's system with a single time constant, representing a homogeneous interface. The system has a solution resistance (R_s), a double layer capacitance (C_{dl}) and a charge transfer resistance (R_{ct}). This corresponding electrical equivalent circuit system was used to fit Nyquist plots results for the uninhibited sample at 20 °C experiments. Fig. 7b represents the second system well fitted with experimental data obtained at 20 °C for the inhibited sample and at 80 °C (Fig. 6) for all samples. The system has a double-time constant, signifying the presence of two layers. The system has a solution resistance (R_s), a film capacitance (C_{fc}), a pore resistance (R_{pr}), a double layer capacitance (C_{dl}) and a charge transfer resistance (R_{ct}). Different circuit element values as shown in Fig. 7 were fitted on the EIS data (Fig. 6) obtained in the solution without and with the initial injection of the alkanolamines at 20 and 80 °C and the results are listed in Table 5. The fitted data are discussed below.

Furthermore, to understand the effect of inhibitor injection on the kinetics of $FeCO_3$ formation, EIS measurements were conducted and the obtained Nyquist data are shown in Fig. 8 at various immersion times. Fig. 8a presents the Nyquist plots for the reference sample, note that an abrupt change in impedance values occurred before 32 hrs, which can be considered as the initial point for the formation of $FeCO_3$ corrosion product. Similarly, Fig. 8b and c show the cases for ethanolamine injected before and after the formation of $FeCO_3$ corrosion products, respectively. In Fig. 8b, when ethanolamine was injected and before the formation of $FeCO_3$, there is a gradual change in the impedance results with time until 52 hrs which is also consistent with LPR results (Fig. 5a), confirming the delay in $FeCO_3$ formation caused by an antagonistic steel surface/inhibitor interaction. However, in the third case when ethanolamine was injected after the formation of $FeCO_3$, the impedance trends were comparable to the reference sample. After 48 hrs, the amplitude for both cases is similar which may indicate a similar protectiveness conferred by the corrosion product layer on both samples. The evolution of various interfaces on the sample surface after the alkanolamine addition can be characterized with the fitted EIS parameters, as typically listed for triethanolamine injection in Table 6, using the equivalent circuit in Fig. 7b, which is commonly used to simulate the surface of an electrode with a top layer having a low conductivity [24,25].

Table 4
Comparison in the inhibition efficiency of the various alkanolamines at different temperatures of 20 °C and 80 °C.

Inhibitor type	Inhibitor efficiency (%) at 20 °C	Inhibitor efficiency (%) at 80 °C
Ethanolamine	46.7	35.5
Diethanolamine	33.1	22.2
Triethanolamine	26.1	6.6

3.3.3. Surface characterizations

Fig. 9 shows the XRD patterns of the corrosion products formed on the specimens during the electrochemical experiments in the 1 wt% NaCl solution. Peaks corresponding to cementite (Fe_3C) were detected in the corrosion products at both 20 °C and 80 °C, whereas, siderite ($FeCO_3$) was only detected on the corroded surface at 80 °C. For injection frequency of the alkanolamines on steel at 20 °C, only Fe_3C was discovered along with the main GIXRD peak corresponding to the martensite. At 80 °C and pH 6.5, both Fe_3C and $FeCO_3$ (siderite) were identified in the GIXRD pattern. The high-intensity peak for siderite which was recorded at 2θ= 48.40° on the corroded samples at 80 °C corresponded to the (104) plane [48].

Fig. 10a, b and c represent cross-sectional SEM images of reference and ethanolamine and triethanolamine samples, respectively, after 24 hrs immersion in the solution at 80 °C. The SEM images show a

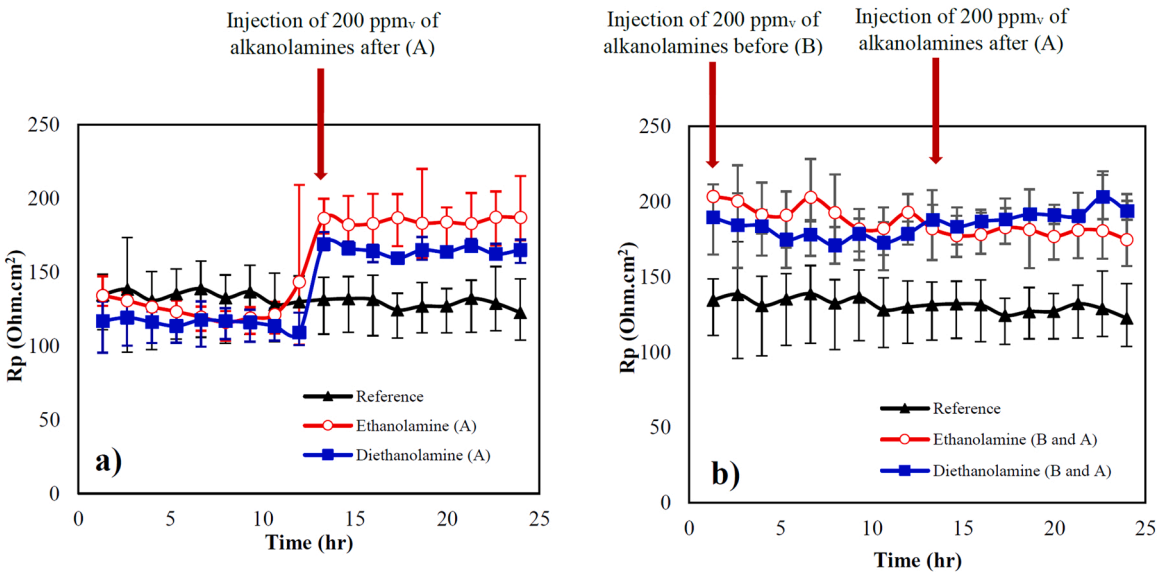

Fig. 4. Variations of polarization resistance vs time for L80–1 Cr steel exposed to 1 wt% NaCl solution at 20 °C, with different types of alkanolamines at 200 ppmv concentration injected (a) injected after 12 hrs (A) and (b) injected initially and after 12 hrs (B and A) for 24 hrs experimental study.

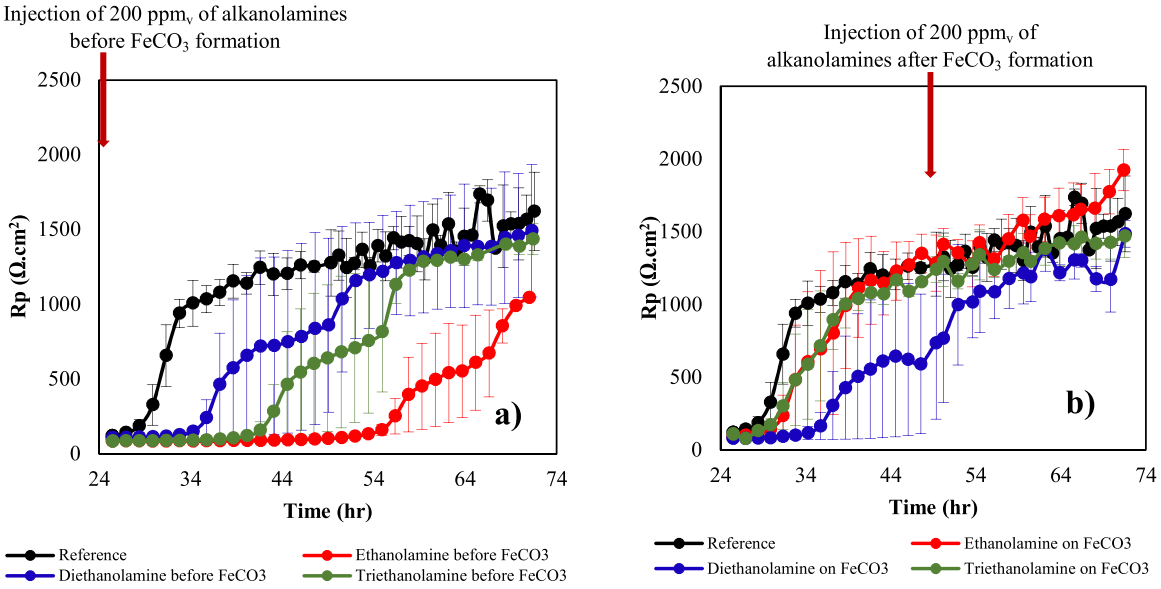

Fig. 5. Variations of polarization resistance vs time for L80–1 Cr steel exposed to 1 wt% NaCl solution at 80 °C, with different types of alkanolamines at 200 ppmv concentration injected (a): before $FeCO_3$ products formation and (b): after $FeCO_3$ formation.

corrosion product layer with a similar thickness of about 30 μm for the samples, while the layers on the reference and triethanolamine samples (Fig. 11a and c) seem to be less dense (more porous) compared with ethanolamine. Fig. 10d typically represents the morphology of the corrosion products formed on the reference sample at 80 °C. The figure shows a layer with prismatic shape crystals covered the surface, which reveals the characteristic feature for iron carbonate as previously reported in the literature [29,49].

Fig. 11 shows the SEM images of the cross-section of the samples after implementing the inhibitor injection frequency cases at a temperature of 20 °C as explained in Fig. 1a. Based on the GIXRD patterns in Fig. 9, at 20 °C, no corrosion products were formed on the surface, and the thin layers presented on the surfaces in Fig. 11 are the Fe_3C that remained after ferrite oxidative dissolution. In Fig. 11a and b, when ethanolamine and diethanolamine were injected after 12 hrs of pre-corrosion, a thin adherent layer of Fe_3C was observed. In Fig. 11c and d, however, when the alkanolamines were injected twice before and after 12 hrs, a more porous and non-adherent layer of Fe_3C is observable. Intermittent (cracked) porosities were also visible within the top layer (Fig. 11a and d).

Fig. 12 shows the cross-sectional and top-view SEM images of the anodically polarized sample exposed to the solution without and with triethanolamine at a temperature of 80 °C and pH 6.5. The EDS elemental maps of iron, carbon and oxygen taken from the cross-section of the sample inhibited by triethanolamine are also prepared in Fig. 12d. The results in Fig. 12 in conjunction with the GIXRD patterns indicate the presence of $FeCO_3$ corrosion products together with a residual Fe_3C network in the samples. Fig. 12a represents the reference sample, which shows a thick layer of $FeCO_3$ corrosion products (approx. 16 μm), where Fe_3C is incorporated between the surrounding $FeCO_3$ corrosion products. Fig. 12b and c represent the sample exposed to triethanolamine after and before the formation of $FeCO_3$ corrosion products,

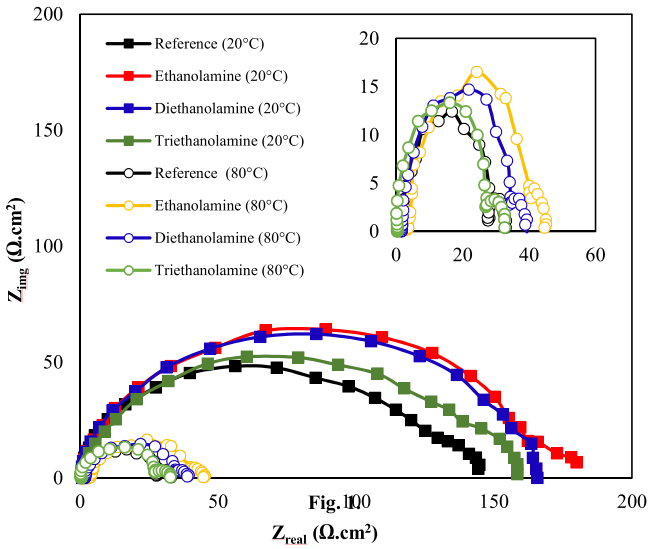

Fig. 6. Results of electrochemical impedance measurements: Nyquist plot for L80–1 Cr steel exposed to 1 wt% NaCl solution at 20 °C and 80 °C, without and with the addition of 200 ppmv of different alkanolamines after 24 hrs.

respectively. When triethanolamine was injected before (Fig. 12c), the $FeCO_3$ corrosion products are more porous and thicker (approx 0.18 μm) compared to the sample exposed with ethanolamine after the layer formation (Fig. 12b).

4. Discussion

The temperature variations between the limiting ranges of 20 – 80 °C in the oil production wells in the Danish sector can significantly change the corrosion resistance of utilized steel tubes. In general terms, the results presented in this paper confirm the importance of the temperature variations as one of the governing factors, which affects both the nature and morphology of the corrosion products, influencing the corrosion behavior of 1Cr steel in a CO_2 environment. The results also showed how the use of the inhibitors and the injection times can alter the corrosion behavior and the kinetics of $FeCO_3$ formation (Figs. 3, 4, 5 and 8). This effect was linked to the characteristics of the $FeCO_3$ layer developed at higher temperatures influencing their protectiveness.

Although amines can act as the pH modifier of the solution, by which the corrosion behavior slightly changes; the basic inhibitive mechanism of amines is that they get chemically adsorbed (chemisorbed) on the steel surface [50,51]. The XPS spectra in Fig. 2 demonstrated that the interaction between the inhibitor and the steel surface is mainly due to the formation of a bond between the N electron pair and the electron cloud at the metal surface. In this interaction, the N-containing functional groups of amines act as the predominant unshared electron pair donors to the electron-depleted dehydrated steel surface [52]. The DFT calculations are consistent with this viewpoint, because the adsorption energies in Table 3 for binding with the nitrogen functional group are stronger than water and the alcohol functional group of the amines. As a

Table 5
EIS parameters obtained based on the fitted curves on experimental data according to equivalent circuit presented in Figs. 7a and 8b for L80–1 Cr steel exposed to 1 wt% NaCl solution at 20 °C and 80 °C, without and with the addition of 200 ppm_v of the different alkanolamines after 24 hrs.

Sample	R_{ct} Ω. cm^2	C_{dl} $\mu\Omega^{-1}$. $cm^{-2}.s^n$	n_1	R_{pr} Ω. cm^2	C_{fc} $\mu\Omega^{-1}$. $cm^{-2}.s^n$	n_2
At the temperature of 20 °C						
Reference	128	1235	0.77	–		
Ethanolamine	19	110×10^3	0.84	170	747	1
Diethanolamine	17	64×10^3	0.85	141	700	0.98
Triethanolamine	12	199×10^3	0.81	136	861	0.99
At the temperature of 80 °C						
Reference	5	646×10^3	1.00	25	1104	0.99
Ethanolamine	12	893×10^3	0.86	31	1168	0.94
Diethanolamine	4	666×10^3	1.00	36	1158	0.95
Triethanolamine	4	632×10^3	0.91	30	1237	0.95

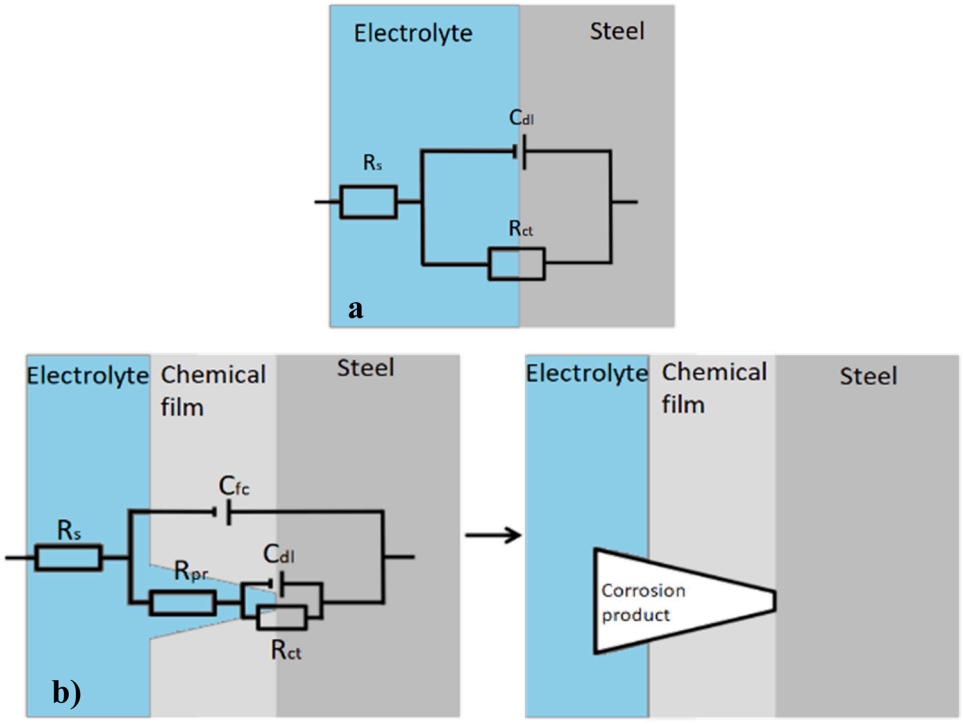

Fig. 7. (a) Simplified Randle's system showing a single layer interface, (b) a double-time constant circuit showing a perforated film interface or perforations filled with corrosion product.

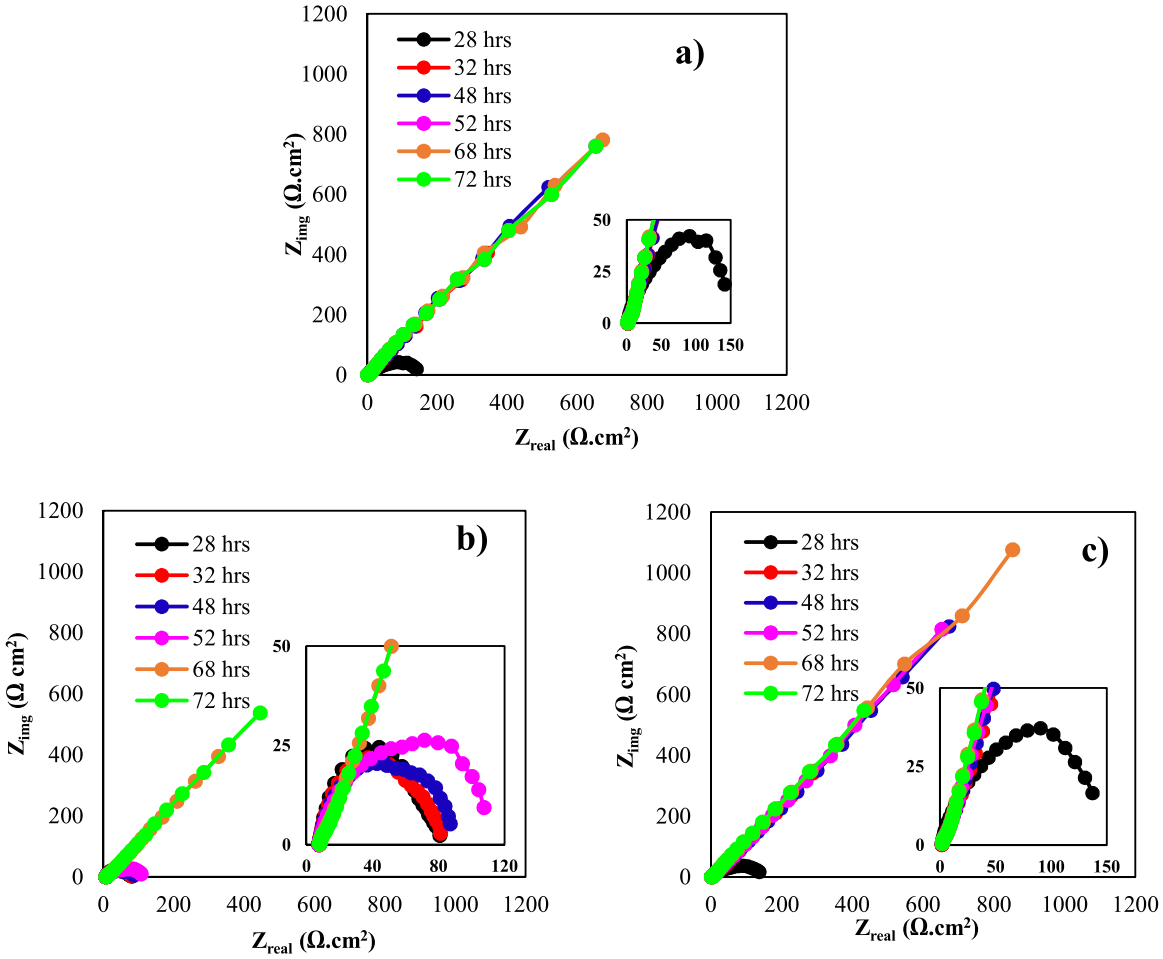

Fig. 8. Nyquist plots at different time intervals for (a) reference sample, (b) ethanolamine injected before the formation of $FeCO_3$ corrosion products and (c) ethanolamine injected after the $FeCO_3$ products were formed; on L80–1 Cr steel in 1 wt% NaCl solution at 80 °C.

Table 6
EIS spectra results based on fitted curves on experimental data obtained at various immersion times according to equivalent circuit in Fig. 7b for injection frequency experiments for L80–1 Cr steel exposed to 1 wt% NaCl solution at 80 °C, with triethanolamine at 200 ppm_v concentration injected before and after the formation of the $FeCO_3$ corrosion products.

Test condition	Immersion time, hrs	R_{ct} Ω.cm²	C_{dl} μΩ^{-1}.cm^{-2}.s^n	n_1	R_{pr} Ω.cm²	C_{fc} μΩ^{-1}.cm^{-2}.s^n	n_2
Triethanolamine injection on $FeCO_3$	28	1466	17158	0.92	363	4489	0.95
	48	1658	15399	1.00	410	4015	1.00
	72	1783	9039	0.92	453	3783	0.86
Triethanolamine injection before $FeCO_3$ formation	28	19	59427	0.79	58	1083	0.95
	48	71	24455	0.87	68	1547	1.00
	72	1732	14097	0.92	432	3121	0.91

result of the strong surface bonds, in particular the negative difference in adsorption energy between the amine and water (Table 3), a durable top layer can potentially be formed and the iron dissolution on the underlying steel substrate can be limited. The calculations are consistent with the alkanolamine binding stronger than water for all surface models. This leads to the establishment of a higher corrosion resistance of 1Cr steel in the alkanolamine−containing NaCl solution as compared to the reference sample (see Fig. 3c, d, e and f). The iron dissolution resulted in a residual Fe_3C layer on the corroded surface (Fig. 11). When the alkanolamines were injected initially and after 12 hrs (Fig. 11c and d), the surface layer was more porous compared to that injected once at the beginning of the experiment (Fig. 11a and b). When the alkanolamines were injected for the first time, they immediately bind at the active sites on the steel surface (adsorption), leading to less iron dissolution. But, the subsequent desorption of the initially injected inhibitors happened after the alkanolamines reinjection could cause the layer detachment as shown in Fig. 11c and d.

However, at the higher temperature (i.e., 80 °C), while the alkanolamines play a role in the morphology of $FeCO_3$ corrosion products (Fig. 12), the efficiency for the alkanolamines is comparatively low (Fig. 3c, d and Table 4). Table 5 shows that there is a difference in R_{ct} values at 20 °C and 80 °C in which the lower R_{ct} value is observed at a temperature of 80 °C. It should be pointed out that the overall adsorption property of nitrogen groups on the steel surface mainly depends on the bulkiness of the attaching groups [39]. But, the groups attached to N in all types of the alkanolamines used in this experiment are not bulky enough to strongly bond with the steel surface. On the other hand, the entropy of molecules adsorbing on a solid surface is about 2/3 of their corresponding gas or liquid phase entropy [53,54]. This means that for small inhibitor molecules, such as alkanolamines, which only replace

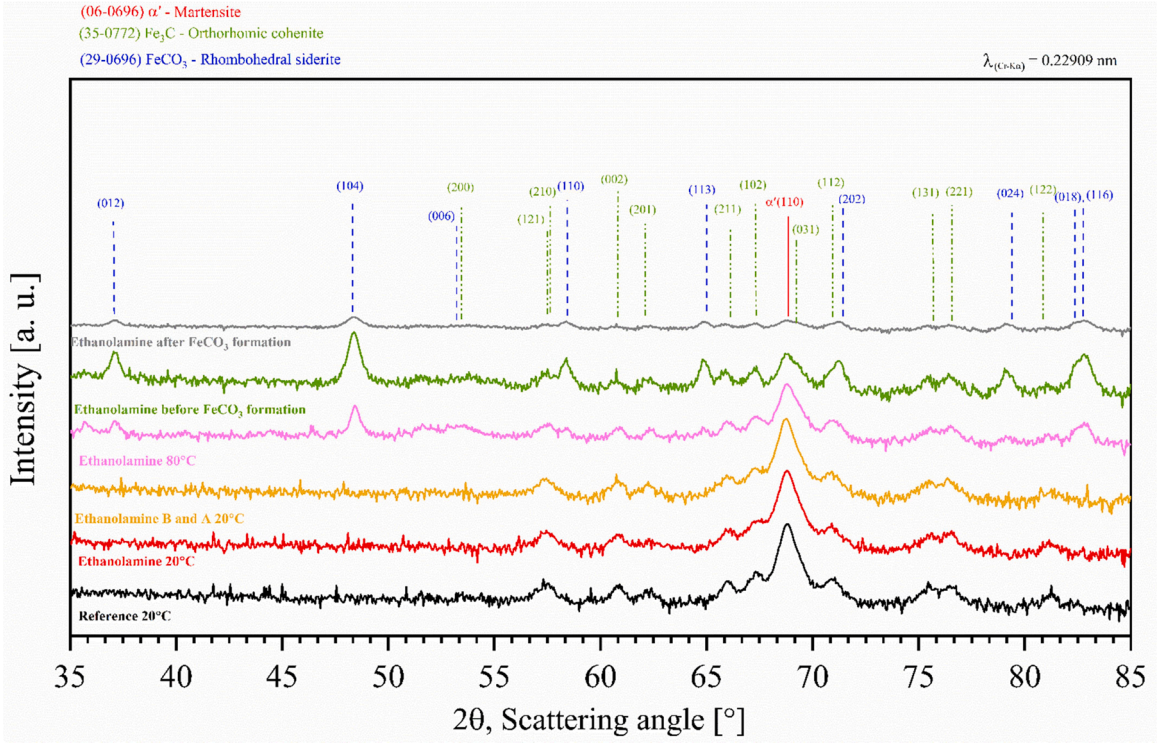

Fig. 9. Grazing incidence X-ray diffraction patterns for the corrosion products formed on steel surface at (a) 20 °C, pH 3.92, (b) 80 °C, pH 4.2 (c) 20 °C and pH 3.92 when alkanolamines were injected before and after 12 hrs, (d): 80 °C, pH 6.5 when alkanolamines were injected before $FeCO_3$ formation and (e): 80 °C, pH 6.5 when the alkanolamines were injected on a pre-formed $FeCO_3$ layer. The Cr-Kα radiation with a wavelength (λ) of 0.22909 nm was used during the GIXRD experiments.

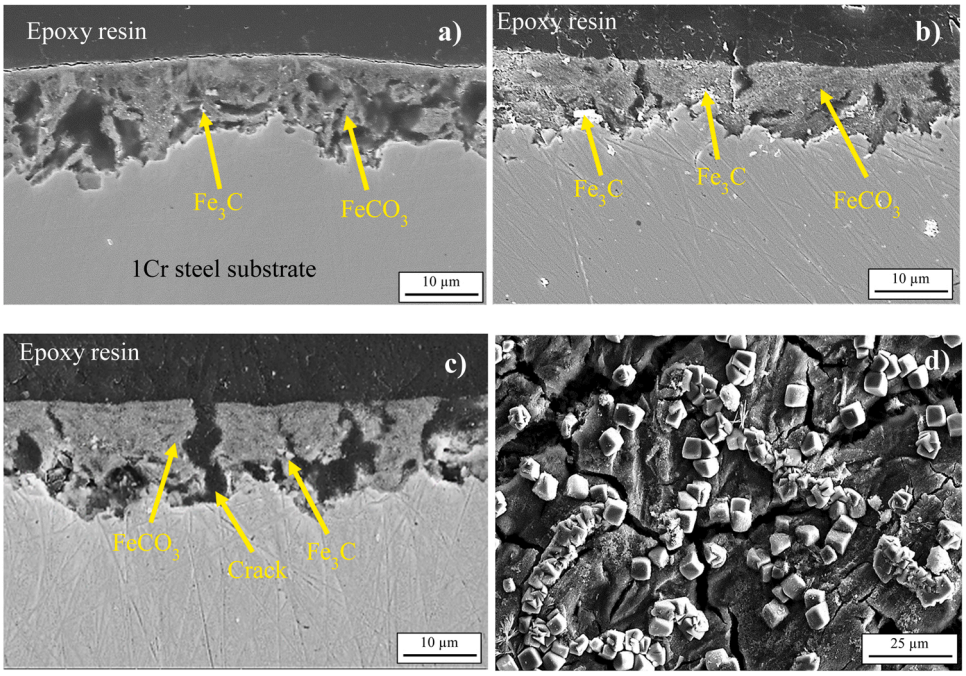

Fig. 10. SEM images for L80–1 Cr steel exposed to 1 wt% NaCl solution, (a): cross-sectional view of the sample without amine injection at 80 °C, (b): cross-sectional view of the sample exposed to the ethanolamine-containing solution at 80 °C, (c): cross-sectional view of the sample exposed to the triethanolamine-containing solution at 80 °C, (d): surface morphology of the reference sample without amine injection at 80 °C.

one (ethanolamine) and one or two (diethanolamine) water molecules from the surface, the entropy of the adsorption is negligible, because the loss of entropy of the adsorbing alkanolamines is almost cancelled by the entropy gaining by desorbing water molecule(s). However, since the alkanolamine molecule is bulkier than the water, the entropy of adsorption can be slightly negative which disfavors the adsorption at the higher temperature. Therefore, the small alkanolamines in this study could easily desorb from the metal surface with time. Especially at elevated temperatures, the adsorption/desorption occurs faster and the free energy of the adsorption is weaker because of the unfavorable

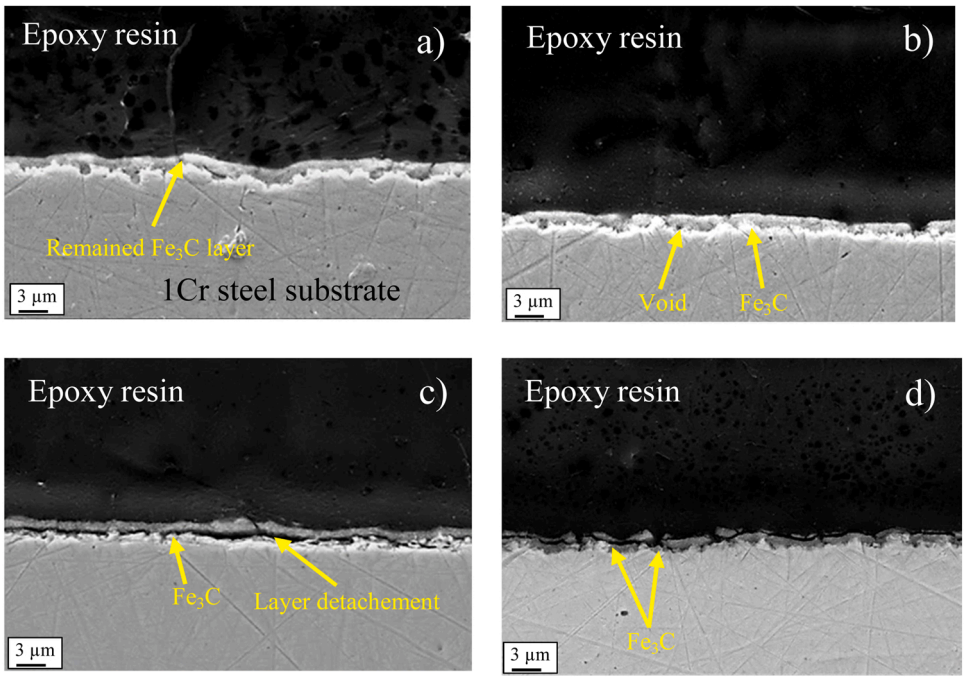

Fig. 11. Cross-sectional SEM images for L80–1 Cr steel exposed to 1 wt% NaCl solution at 20 °C, (a) ethanolamine injected after 12 hrs of the immersion, (b) diethanolamine injected after 12 hrs of the immersion, (c) ethanolamine injected before and after 12 hrs of the experiment, (d) diethanolamine injected before and after 12 hrs of the experiment.

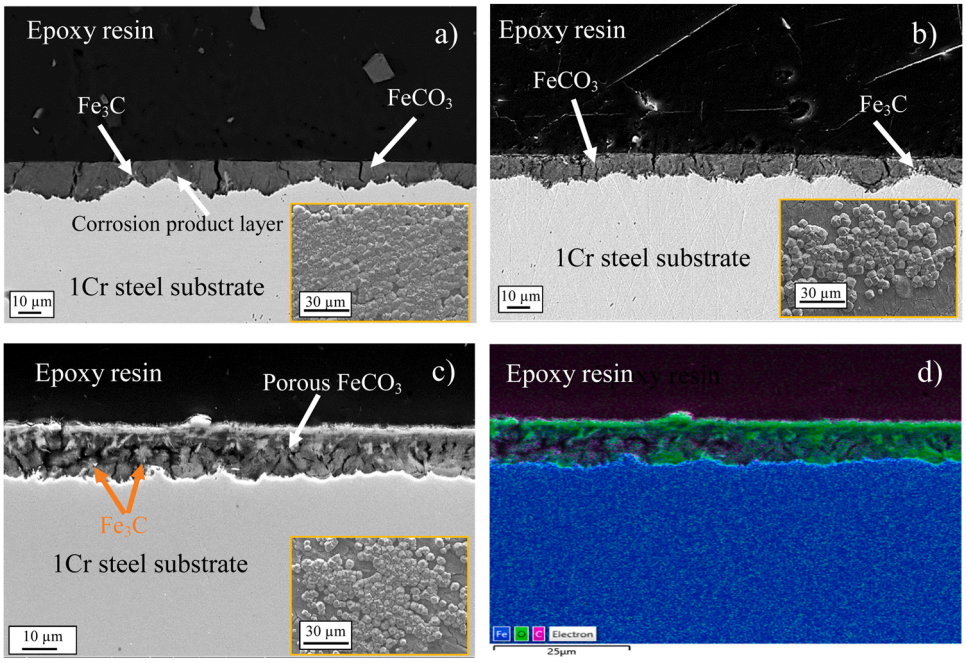

Fig. 12. Cross-sectional SEM images for L80–1 Cr steel exposed to 1 wt% NaCl solution at 80 °C; (a) without alkanolamines injection, (b) with triethanolamine injected on $FeCO_3$ corrosion products, (c) with triethanolamine injected before $FeCO_3$ corrosion products formation. The top view images are also inserted in the figures (d) EDS elemental map of iron, carbon and oxygen taken from the cross-section of the sample inhibited by triethanolamine presented in Fig. 12c.

entropy of adsorption. The easy desorption of the alkanolamines molecules from the surface resulted in a less corrosion inhibition at the higher temperature. Consequently, when the electrochemical conditions were provided for iron carbonate precipitation, a porous layer was formed (Fig. 12c). Therefore, the $FeCO_3$ layers did not provide any kind of protection to the steel surface (Fig. 5). As a result, the solution could readily penetrate the porosities and continued the dissolution of the underlying steel layer.

The calculated adsorption energy for ethanolamine is less negative than diethanolamine (see, Table 3). The reason is that the more bulky group attached to the N atom, the more the steric effect can be, leading to a weaker bond between amines and the steel surface. It means that among the different alkanolamines used in this study, ethanolamine has the less negative absorption energy level due to the nature of the attaching group to the N atom (−NH). However, the results show the highest R_{ct} value (Fig. 3 and Table 5) and efficiency (Table 4) for

ethanolamine, which is in contradiction to its absorption energy level. It is believed that depending on the size of the inhibitor molecules, water can be replaced from the steel surface by the inhibitor molecule, leading to a net increase in entropy, which in turn would lead to stronger binding. This has been observed e.g. for the amphiphilic molecule TOFA/DETA imidazoline molecule [55]. The bonding geometries of the inhibitor molecules on the Fe(110), $Fe_3C(001)$ and $FeCO_3(104)$ planes are presented in Fig. 13a-j. Generally, the atomic-scale distance between inhibitor molecules and those of the substrate provides an appropriate condition for the chemical bonding. The chemical structure of ethanolamine and diethanolamine bonded on the surface with the N-containing functional group is also schematically shown in Fig. 13k and l, respectively. Since ethanolamine has a single linear arrangement of atoms, if two molecules of ethanolamine cover the sample surface, then the gap between both molecules is not enough (Fig. 13k) for the water molecule in come to contact with the sample surface on both Fe(110) (i.e., anode site) and $Fe_3C(001)$ (cathode site) as shown in Fig. 13b and f, respectively. This limits the exposed areas of the surface to the solution and provides a better efficiency for corrosion inhibition. However, in the case of diethanolamine in Fig. 13l, the gap between two diethanolamine molecules is big enough for the water molecule to go in and contact with the sample surface. This means that although diethanolamine more strongly binds with the Fe surface, it results in a poorer corrosion resistance than ethanolamine, due to the interference of water molecules against the performance of diethanolamine.

In Table 3, the adsorption energy values for all three alkanolamines bonded to $FeCO_3$ corrosion products is similar regardless of the bonding geometries of the different inhibitor molecules on $FeCO_3(104)$ in Fig. 13.

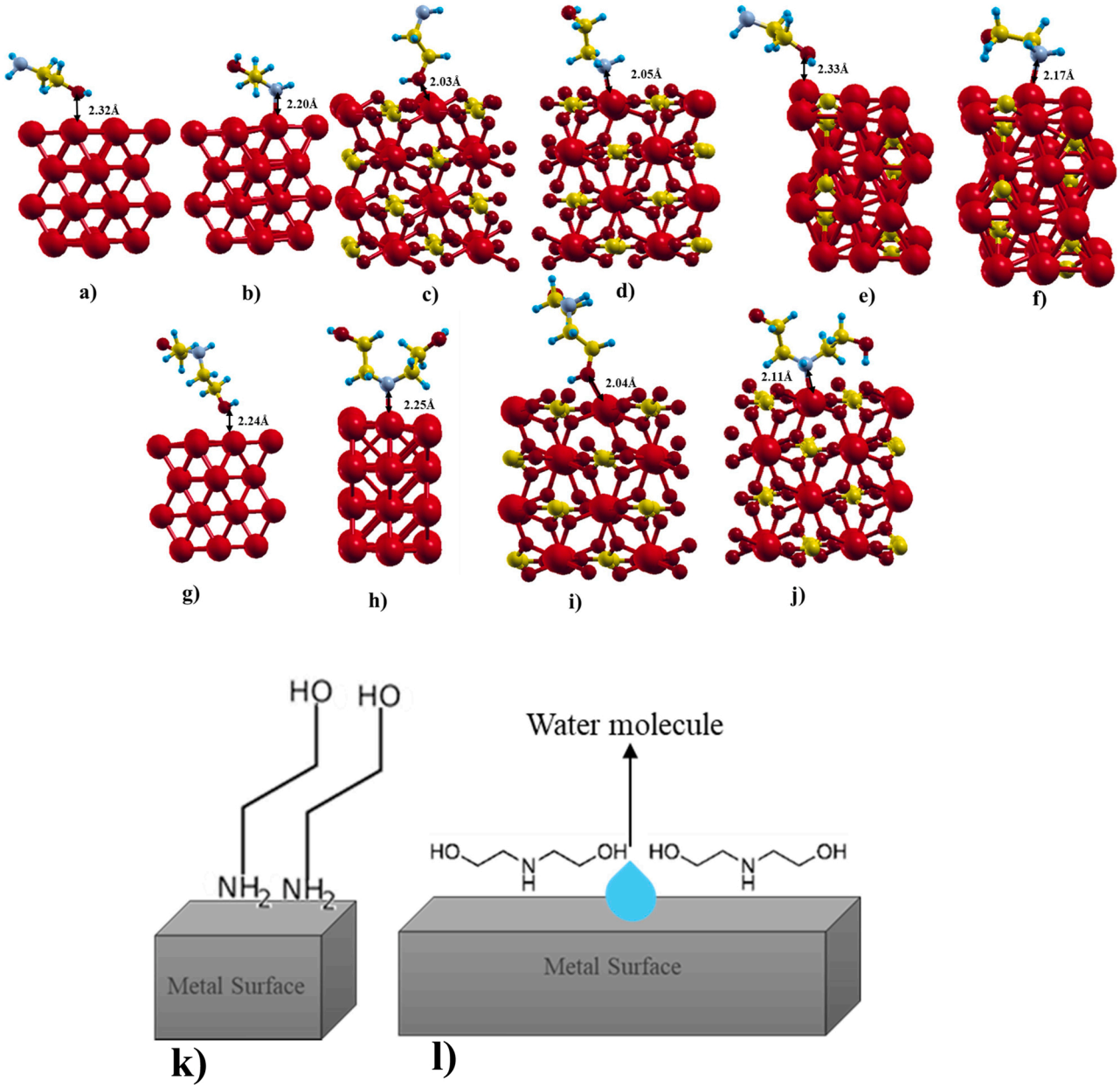

Fig. 13. Optimized bonding geometries for some inhibitor molecules on various model surfaces (a-j) and schematic view of packing efficiency difference between ethanolamine and diethanolamine (k-l). The bonding geometries are: ethanolamine bonded to (a) Fe(110) with -OH, (b) Fe(110) with $-NH_2$, (c) $FeCO_3(104)$ with $-OH$, (d) $FeCO_3(104)$ with $-NH_2$ group, (e) $Fe_3C(001)$ with $-OH$, (f) $Fe_3C(001)$ with $-NH_2$; diethanolamine bonded to: (g) Fe(110) with $-OH$, (h) Fe(110) with $-NH$ group, (i) $FeCO_3(104)$ with $-OH$, (j) $FeCO_3(104)$ with $-NH$. The color code: bright red (large radius) = Fe, dark red (small radius) = O, blue-grey = N, yellow = C, aqua= H.

This led to no significant difference in the polarization resistance value after the injection of alkanolamines (Fig. 5b). For the samples with the pre-formed $FeCO_3$ top layer, the C_{fc} values in Table 6 gradually decreased, which indicates the further precipitation of the $FeCO_3$ layer as reported by Farelas et al. [56]. The C_{fc} decrease has been linked to the layer becoming denser and less porous [57], as confirmed by the increasing values of R_{pr} (see, Table 6), which also is consistent with the corrosion rate obtained by LPR with time (Fig. 5b). On the other hand, the solution could have penetrated the porosities and continued the dissolution of the underlying steel reflected by the decrease in C_{dl}. The slight increase in R_{ct} with time from 1466 $\Omega.cm^2$ to 1658 $\Omega.cm^2$ suggests that the precipitated $FeCO_3$ may have still given some degree of protection. However, the increase is too low for claiming a further protectiveness by this layer, and the fitted data confirm the LPR corrosion rate observed in Fig. 5a, which was almost constant.

However, when the alkanolamines were injected on the steel surface from the beginning of the experiment at the higher temperature, its molecules cover the metal surface and the saturation of Fe^{2+} is postponed to a longer time, thus the limited dissolution of the underlying steel layer continues as reflected by the decrease in C_{dl} with time (Table 6). Due to the absence of a protective corrosion product layer, R_{ct} insignificantly increased from the initial value of 19 $\Omega.cm^2$ to 71 $\Omega.cm^2$ after the immersion time of 48 hrs. Furthermore, once the solution was saturated with Fe^{2+}, the iron carbonate was formed on the surface sites other than those areas blocked by the triethanolamine, leading to a significant R_{ct} increase to 1732 $\Omega.cm^2$ after 72 hrs (Table 6). Later on, the triethanolamine desorption from the surface during $FeCO_3$ formation caused the generation of porosity within the corrosion product layer (Fig. 12c) [58].

5. Conclusions

Different electrochemical methods along with molecular modelling were used to study the effect of temperature (20 °C and 80 °C) on L80–1 Cr steel in the CO_2-saturated 1 wt% NaCl electrolyte without and with the injection of different types of alkanolamines. The following main conclusions were drawn from this study:

- The chemical structures of the alkanolamines and adsorption energy of both Fe(110) and $FeCO_3$(104) played determining role in efficiently inhibiting the corrosion occurrence. Among the alkanolamines, ethanolamine had the best efficiency compared to the other alkanolamines, increasing the R_p value by about 70%.
- The DFT modelling showed that the observed inhibitor efficiency for the ethanolamine and diethanolamine correlated with the adsorption energy of the inhibitors on the model surfaces. Ethanolamine adsorption energy compared to water adsorption energy was favorable on all model surfaces. Ethanolamine was found to be significantly better at replacing water than diethanolamine was on the surface of the corrosion product $FeCO_3$.
- The temperature of the solution also plays a role in the inhibitor efficiency of the alkanolamines. At the higher temperature, there was a lower efficiency of alkanolamines inhibitors, due to higher corrosion kinetics and more desorption of alkanolamines from the surfaces.
- The formation of the corrosion products ($FeCO_3$) was postponed due to the alkanolamine injection. When the alkanolamines were injected at the beginning of the experiment, a porous $FeCO_3$ corrosion product layer was formed, leading to a lower polarization resistance value.
- In the cases of injection frequencies, the reinjection of the alkanolamines did not provide more protectiveness than that by the pre-formed $FeCO_3$ layer.

CRediT authorship contribution statement

Shivangi Gupta: Conceptualization, Methodology, Investigation, Formal analysis, Writing - Original Draft, **Kapil Kumar Gupta:** Methodology, Investigation, Formal analysis, **Martin Andersson:** Validation, Writing - Original Draft, Writing - Review & Editing, Supervision, **Rouhollah Yazdi:** Conceptualization, Formal analysis, Supervision, Writing - Original Draft, Writing - Review & Editing, **Rajan Ambat:** Conceptualization, Supervision, Writing - Review & Editing, Project administration.

Declaration of Competing Interest

The authors declare that they have no known competing financial interests or personal relationships that could have appeared to influence the work reported in this paper.

Acknowledgements

The authors would like to thank the Danish Hydrocarbon Research and Technology Center (DHRTC) for providing financial funding and technical supports to this work. The Mechanical Engineering Department at the Technical University of Demark is appreciatively acknowledged.

References

[1] M.B. Kermani, A. Morshed, Carbon dioxide corrosion in oil and gas production—A compendium, Corros. Sci. Eng. 59 (2003) 659–683.
[2] C. De Waard, D.E. Milliams, Carbonic acid corrosion of steel, Corrosion 31 (1975) 177–181.
[3] R.H. Hausler, H.P. Gaddart, Advances in CO2 corrosion vol. 1, Houston TX, 1985.
[4] R.H. Hausler, H.P. Gaddart, Advances in CO2 corrosion vol. 2, Houston TX, 1986.
[5] M. Rogowska, J. Gudme, A. Rubin, K. Pantleon, R. Ambat, Effect of Fe ion concentration on fatigue life of carbon steel in aqueous CO_2 environment, Corros. Eng. Sci. Technol. 51 (2016) 90–103.
[6] M. Rogowska, J. Gudme, A. Rubin, K. Pantleon, R. Ambat, Effect of Fe ion concentration on corrosion of carbon steel in CO_2 environment, Corros. Eng. Sci. Technol. 51 (2016) 25–36.
[7] S. Nešić, Key issues related to modelling of internal corrosion of oil and gas pipelines - A review, Corros. Sci. 49 (2007) 4308–4338.
[8] A. Kahyarian, B. Brown, S. Nesic, Mechanism of CO2 corrosion of mild steel: A new narrative, in: NACE - Int. Corros. Conf. Ser., 2018: pp. 1–16.
[9] T. das, C. Almeida, M.C.E. Bandeira, R.M. Moreira, O.R. Mattos, New insights on the role of CO_2 in the mechanism of carbon steel corrosion, Corros. Sci. 120 (2017) 239–250.
[10] H. Fang, S. Nesic, B. Brown, S. Wang, General CO2 corrosion in high salinity brines, in: NACE - Int. Corros. Conf. Ser., 2006: pp. 1–15.
[11] M. Nordsveen, S. Nešić, R. Nyborg, A. Stangeland, A mechanistic model for carbon dioxide corrosion of mild steel in the presence of protective iron carbonate films - Part 1: Theory and verification, Corrosion 59 (2003) 443–456.
[12] S. Nešic, M. Nordsveen, R. Nyborg, A. Stangeland, A mechanistic model for carbon dioxide corrosion of mild steel in the presence of protective iron carbonate films—part 2: a numerical experiment, Corrosion 59 (2003) 489–497.
[13] D.A. López, W.H. Schreiner, S.R. De Sánchez, S.N. Simison, The influence of carbon steel microstructure on corrosion layers: An XPS and SEM characterization, Appl. Surf. Sci. 207 (2003) 69–85.
[14] Z.D. Cui, S.L. Wu, C.F. Li, S.L. Zhu, X.J. Yang, Corrosion behavior of oil tube steels under conditions of multiphase flow saturated with super-critical carbon dioxide, Mater. Lett. 58 (2004) 1035–1040.
[15] M.B. Valcarce, M. Vázquez, Carbon steel passivity examined in alkaline solutions: The effect of chloride and nitrite ions, Electrochim. Acta 53 (2008) 5007–5015.
[16] W. Sun, K. Chokshi, S. Nesic, D.A. Gulino, A study of protective iron carbonate scale formation in CO 2 corrosion, AIChE Annu. Meet. Conf. Proc. (2004) 5063–5071.
[17] J.B. Sun, G.A. Zhang, W. Liu, M.X. Lu, The formation mechanism of corrosion scale and electrochemical characteristic of low alloy steel in carbon dioxide-saturated solution, Corros. Sci. 57 (2012) 131–138.
[18] T. Li, Y. Yang, K. Gao, M. Lu, Mechanism of protective film formation during CO_2 corrosion of X65 pipeline steel, J. Univ. Sci. Technol. Beijing Miner. Metall. Mater. (Eng. Ed.). 15 (2008) 702–706.
[19] W. Sun, S. Nešić, Kinetics of corrosion layer formation: Part 1 - Iron carbonate layers in carbon dioxide corrosion, Corrosion 64 (2008) 334–346.
[20] V. Ruzic, M. Veidt, S. Nešić, Protective iron carbonate films -Part 2: Chemical removal by dissolution in single-phase aqueous flow, Corrosion 62 (2006) 598–611.

[21] V. Ruzic, M. Veidt, S. Nešić, Protective iron carbonate films - Part 3: Simultaneous chemo-mechanical removal in single-phase aqueous flow, Corrosion 63 (2007) 758–769.

[22] V. Ruzic, M. Veidt, S. Nešić, Protective iron carbonate films — Part 1: Mechanical removal in single-phase aqueous flow, Corrosion 62 (2006) 419–432.

[23] S. Wang, K. George, S. Nesic, High pressure CO_2 corrosion electrochemistry and the effect of acetic acid, Corrosion (2004) 1–17.

[24] K. George, S. Nesic, C. De Waard, Electrochemical investigation and modeling of carbon dioxide corrosion of carbon steel in the presence of acetic acid, in: NACE Meet. Pap., 2004: pp. 1–25.

[25] Z.F. Yin, Y.R. Feng, W.Z. Zhao, Z.Q. Bai, G.F. Lin, Effect of temperature on CO_2 corrosion of carbon steel, Surf. Interface Anal. 41 (2009) 517–523.

[26] M.B. Tomson, M.L. Johnson, How ferrous carbonate kinetics impacts oilfield corrosion, Soc. Pet. Eng. (1991) 257–264.

[27] F. de Moraes, J.R. Shadley, J. Chen, E.F. Rybicki, Characterization of CO_2 corrosion product scales related to environmental conditions, Corrosion (2000).

[28] A. Munoz, J. Genesca, R. Duran, J. Mendoza, Mechanism of FeCO3 formation on API X70 pipeline steel in brine solutions containing CO_2, Proc. Corros. (2005) 1–14.

[29] A. Dugstad, Mechanism of protective film formation during CO_2 corrosion of carbon steel, Corrosion (1998) 1–11.

[30] B.M. Miksic, A.Y. Furman, M.A. Kharshan, Effectiveness of the corrosion inhibitors for the petroleum industry under various flow conditions, in: NACE - Int. Corros. Conf. Ser., 2009: pp. 1–9.

[31] M.N. Rahuma, M.B. EL-Sabbah, I.M. Hamad, Effect of serine and methionine on electrochemical behavior of the corrosion of mild steel in aqueous solutions, ISRN Corros. (2013) 1–7.

[32] I. Jevremović, V. Mišković-Stanković, The inhibitive effect of ethanolamine on corrosion behavior of aluminium in NaCl solution saturated with CO_2, Metall, Mater. Eng. 18 (2012) 241–257.

[33] I.C. Ivonye, Corrosion processes and mechanisms in the presence of monoethylene glycol (MEG), The University of Leeds, 2014.

[34] M.P. Desimone, G. Gordillo, S.N. Simison, The effect of temperature and concentration on the corrosion inhibition mechanism of an amphiphilic amido-amine in CO_2 saturated solution, Corros. Sci. 53 (2011) 4033–4043.

[35] K. Xhanari, N. Grah, M. Finšgar, R. Fuchs-Godec, U. Maver, Corrosion inhibition and surface analysis of amines on mild steel in chloride medium, Chem. Pap. 71 (2017) 81–89.

[36] R. Rihan, R. Shawabkeh, N. Al-Bakr, The effect of two amine-based corrosion inhibitors in improving the corrosion resistance of carbon steel in sea water, J. Mater. Eng. Perform. 23 (2014) 693–699.

[37] P. Giannozzi, S. Baroni, N. Bonini, M. Calandra, R. Car, C. Cavazzoni, D. Ceresoli, G.L. Chiarotti, M. Cococcioni, I. Dabo, A. Dal Corso, S. de Gironcoli, S. Fabris, G. Fratesi, R. Gebauer, U. Gerstmann, C. Gougoussis, A. Kokalj, M. Lazzeri, L. Martin-Samos, N. Marzari, F. Mauri, R. Mazzarello, S. Paolini, A. Pasquarello, L. Paulatto, C. Sbraccia, S. Scandolo, G. Sclauzero, A.P. Seitsonen, A. Smogunov, P. Umari, R.M. Wentzcovitch, QUANTUM ESPRESSO: a modular and open-source software project for quantum simulations of materials, J. Phys. Condens. Matter (2009) 1–36.

[38] Y. Zhang, W. Yang, Comment on "generalized gradient approximation made simple,", Phys. Rev. Lett. 80 (1998) 890.

[39] M.P. Andersson, Density functional theory with modified dispersion correction for metals applied to self-assembled monolayers of thiols on Au(111), J. Theor. Chem. (2013) 1–9.

[40] S. Grimme, Semiempirical GGA-type density functional constructed with a long-range dispersion correction, J. Comput. Chem. 27 (2006) 1787–1799.

[41] V. Barone, M. Casarin, D. Forrer, M. Pavone, M. Sambi, A. Vittadini, Role and effective treatment of dispersive forces in materials: Polyethylene and graphite crystals as test cases, J. Comput. Chem. 30 (2009) 934–939.

[42] S. Ehrlich, J. Moellmann, W. Reckien, T. Bredow, S. Grimme, System-dependent dispersion coefficients for the DFT-D3 treatment of adsorption processes on ionic surfaces, ChemPhysChem 12 (2011) 3414–3420.

[43] E. Ataman, M.P. Andersson, M. Ceccato, N. Bovet, S.L.S. Stipp, Functional group adsorption on calcite: I. oxygen containing and nonpolar organic molecules, J. Phys. Chem. C. 120 (2016) 16586–16596.

[44] E. Ataman, M.P. Andersson, M. Ceccato, N. Bovet, S.L.S. Stipp, Functional group adsorption on calcite: II. Nitrogen and sulfur containing organic molecules, J. Phys. Chem. C. 120 (2016) 16597–16607.

[45] A. Dal, Corso, Pseudopotentials periodic table: From H to Pu, Comput. Mater. Sci. 95 (2014) 337–350.

[46] A. Dal Corso, PSlibrary: A library of ultrasoft and PAW pseudopotentials, (2020).

[47] M.A. Amin, S.S. Abd El-Rehim, E.E.F. El-Sherbini, R.S. Bayoumi, The inhibition of low carbon steel corrosion in hydrochloric acid solutions by succinic acid: Part I. Weight loss, polarization, EIS, PZC, EDX and SEM studies, Electrochim. Acta 52 (2007) 3588–3600.

[48] R. Rizzo, S. Gupta, M. Rogowska, R. Ambat, Corrosion of carbon steel under CO_2 conditions: Effect of CaCO3 precipitation on the stability of the FeCO3 protective layer, Corros. Sci. 162 (2020) 1–12.

[49] A. Dugstad, Fundamental aspects of CO_2 metal loss corrosion, Part I: mechanism, Corrosion (2015) 1–12.

[50] L. Bin Zhao, R. Huang, M.X. Bai, D.Y. Wu, Z.Q. Tian, Effect of aromatic amine-metal interaction on surface vibrational Raman spectroscopy of adsorbed molecules investigated by density functional theory, J. Phys. Chem. C. 115 (2011) 4174–4183.

[51] G. Banerjee, S.N. Malhotra, Contribution to adsorption of aromatic amines on mild steel surface from HCl solutions by impedance, UV, and Raman spectroscopy, Corrosion 48 (1992) 10–15.

[52] N. Goudarzi, M. Peikari, M. Reza Zahiri, H. Reza Mousavi, Adsorption and corrosion inhibition behavior of stainless steel 316 by aliphatic amine compounds in acidic solution, Arch. Metall. Mater. 57 (2012) 845–851.

[53] C.T. Campbell, J.R.V. Sellers, The entropies of adsorbed molecules, J. Am. Chem. Soc. 134 (2012) 18109–18115.

[54] A. Budi, S.L.S. Stipp, M.P. Andersson, Calculation of entropy of adsorption for small molecules on mineral surfaces, J. Phys. Chem. C. 122 (2018) 8236–8243.

[55] I. Jevremović, M. Singer, S. Nešić, V. Miskovic-Stanković, Inhibition properties of self-assembled corrosion inhibitor talloil diethylenetriamine imidazoline for mild steel corrosion in chloride solution saturated with carbon dioxide, Corros. Sci. 77 (2013) 265–272.

[56] F. Farelas, M. Galicia, B. Brown, S. Nesic, H. Castaneda, Evolution of dissolution processes at the interface of carbon steel corroding in a CO_2 environment studied by EIS, Corros. Sci. 52 (2010) 509–517.

[57] C. Liu, Q. Bi, A. Leyland, A. Matthews, An electrochemical impedance spectroscopy study of the corrosion behavior of PVD coated steels in 0.5 N NaCl aqueous solution: part I. Establishment of equivalent circuits for EIS data modelling, Corros. Sci. 45 (2003) 1243–1256.

[58] C. Liu, Q. Bi, A. Leyland, A. Matthews, An electrochemical impedance spectroscopy study of the corrosion behavior of PVD coated steels in 0.5 N NaCl aqueous solution: Part II. EIS interpretation of corrosion behaviour, Corros. Sci. 45 (2003) 1257–1273.